

CO ICE PHOTODESORPTION: A WAVELENGTH-DEPENDENT STUDY

EDITH C. FAYOLLE¹, MATHIEU BERTIN², CLAIRE ROMANZIN^{2,4}, XAVIER MICHAUT², KARIN I. ÖBERG³,
HAROLD LINNARTZ¹, AND JEAN-HUGUES FILLION²

¹ Sackler Laboratory for Astrophysics, Leiden Observatory, Leiden University, P.O. Box 9513, 2300 RA Leiden, The Netherlands

² Laboratoire de Physique Moléculaire pour l'Atmosphère et l'Astrophysique, Université Pierre et Marie Curie-Paris 6, CNRS UMR7092, 75005 Paris, France

³ Harvard-Smithsonian Center for Astrophysics, 60 Garden Street, Cambridge, MA 02138, USA

Received 2011 June 10; accepted 2011 August 3; published 2011 August 30

ABSTRACT

UV-induced photodesorption of ice is a non-thermal evaporation process that can explain the presence of cold molecular gas in a range of interstellar regions. Information on the average UV photodesorption yield of astrophysically important ices exists for broadband UV lamp experiments. UV fields around low-mass pre-main-sequence stars, around shocks and in many other astrophysical environments are however often dominated by discrete atomic and molecular emission lines. It is therefore crucial to consider the wavelength dependence of photodesorption yields and mechanisms. In this work, for the first time, the wavelength-dependent photodesorption of pure CO ice is explored between 90 and 170 nm. The experiments are performed under ultra high vacuum conditions using tunable synchrotron radiation. Ice photodesorption is simultaneously probed by infrared absorption spectroscopy in reflection mode of the ice and by quadrupole mass spectrometry of the gas phase. The experimental results for CO reveal a strong wavelength dependence directly linked to the vibronic transition strengths of CO ice, implying that photodesorption is induced by electronic transition (DIET). The observed dependence on the ice absorption spectra implies relatively low photodesorption yields at 121.6 nm ($\text{Ly}\alpha$), where CO barely absorbs, compared to the high yields found at wavelengths coinciding with transitions into the first electronic state of CO ($\text{A}^1\Pi$ at 150 nm); the CO photodesorption rates depend strongly on the UV profiles encountered in different star formation environments.

Key words: astrochemistry – ISM: abundances – ISM: molecules – molecular data – molecular processes

Online-only material: color figure

1. INTRODUCTION

Carbon monoxide, the second most abundant molecule observed in the gas phase of the interstellar medium (ISM) after H_2 , is also one of the most commonly detected molecules in the solid phase, condensed on the surface of sub-micron size dust grains (e.g., Pontoppidan et al. 2003). Mechanisms triggering CO phase transitions under densities and temperatures encountered in star-forming environments are crucial to interpret observations of CO lines. In cold parts of the ISM, most of the CO is depleted onto the grains but non-thermal desorption mechanisms, such as UV photodesorption or cosmic ray sputtering, can maintain a part of the CO budget in the gas phase, explaining the presence of CO below its thermal desorption temperature (e.g., Willacy & Langer 2000).

Desorption of CO ice induced by UV photons under astrophysically relevant conditions has recently been studied by Öberg et al. (2007, 2009), and Muñoz Caro et al. (2010) using an H_2 based broadband microwave discharge lamp as photon source and monitoring the ice loss through infrared spectroscopy during irradiation. The derived photodesorption rates are substantially higher than previously assumed (Greenberg 1973), but differ by up to a factor of 20 between the two groups. Absolute photodesorption yield values have substantial uncertainties resulting from (1) the different photon flux calibration—Öberg et al. (2007, 2009) used a NIST-calibrated photodiode whereas Muñoz Caro et al. (2010) employed a chemical actionometry method—and (2) the IR measurement of the ice sublimation,

performed in transmission in the case of Muñoz Caro et al. (2010), and in reflection in the case of Öberg et al. (2007, 2009). Nonetheless, the combined uncertainties are estimated to a factor of a few and cannot fully account for the order of magnitude difference between the two groups. The different UV irradiation profiles of the two discharge lamps may instead be at the origin of this discrepancy if the photodesorption efficiency is wavelength dependent.

From these studies, excitation of CO in its first electronic state was proposed to induce desorption after energy transfer to neighboring CO molecules and rearrangement of the ice surface (M. C. van Hemert 2010, private communication). Wavelength-resolved studies are required to confirm this mechanism and to investigate whether the photodesorption mechanism of CO is wavelength dependent.

Wavelength-resolved photodesorption yields are also important for astrochemical networks. Different FUV field profiles are encountered at different star formation stages and around young stellar objects of different spectral types. The FUV can be dominated by the interstellar radiation field (ISRF) at the edge of molecular clouds, cosmic-rays excited H_2 emission in starless clouds (Gredel et al. 1987), black body emission from protostars, and emission lines due to material accretion onto the protostar or pre-main-sequence star (Bergin et al. 2003; van Dishoeck et al. 2006). Thus if photodesorption yields are wavelength-dependent, the photodesorption yield per incident UV photon may vary significantly in different star-forming environments.

In order to fully characterize the CO photodesorption process, the present work investigates for the first time the wavelength dependence of CO photodesorption yields for astrophysically

⁴ Current address: Laboratoire de Chimie Physique, Université Paris Sud 11, CNRS UMR 8000, 91405 Orsay, France.

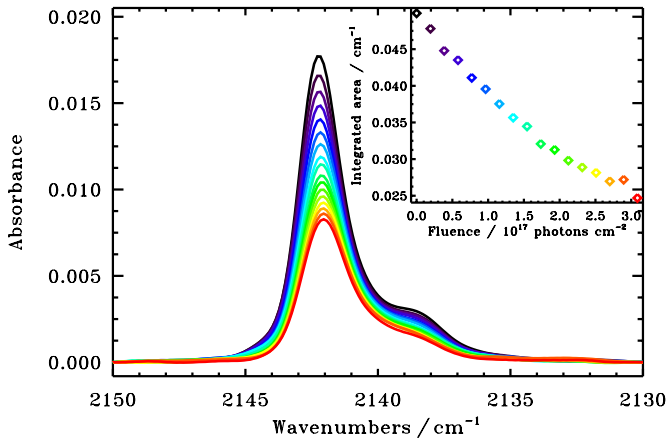


Figure 1. Decrease of the CO vibration RAIRS signal during irradiation of a CO ice 10 ML thick at 18 K by 9.2 eV photons. Inset shows the integrated area of the corresponding CO RAIRS band vs. UV fluence.

(A color version of this figure is available in the online journal.)

relevant ices and conditions. The experimental techniques for ice preparation and synchrotron-based irradiations are explained in Section 2. The results are described in Section 3 and the mechanism and astrophysical implications are discussed in Section 4.

2. EXPERIMENTAL

CO ices are grown and irradiated in the SPICES (Surface Processes in ICES) apparatus, described in detail elsewhere (Bertin et al. 2011). CO ice films are prepared under ultra high vacuum (UHV) conditions (base pressure: 5×10^{-10} Torr) on a polycrystalline gold substrate which is cooled down to 18 K by a closed cycle helium cryostat. The CO ices are grown via background deposition, i.e., by exposing the cold Au surface to a partial pressure of CO gas (Air Liquide, 99% purity) during a given time. The amount of CO deposited on the surface is monitored through Reflection Absorption InfraRed Spectroscopy (RAIRS). The thickness of the deposited ice in monolayers (ML) is obtained by performing an isothermal desorption experiment of the CO ice monitored by RAIRS, resulting in the absorbance of 1 ML of CO ice (Öberg et al. 2009). Complementary estimations of the CO ice thickness have also been performed using temperature-programmed desorption experiments and from the exposure, assuming a sticking coefficient of unity. All techniques gave similar results, yielding ice thicknesses between 9 and 10 ML.

The set-up is equipped with two complementary photodesorption detection techniques. A Quadrupole Mass Spectrometer (QMS) allows the detection of gas-phase molecules within the UHV chamber, while condensed molecules are probed by RAIRS. Simultaneous probing of the remaining condensed molecules and of the gas-phase photodesorbed molecules is therefore possible during ice irradiation. QMS measurements are used to determine the relative photodesorption rates for all employed UV fluxes, while RAIRS provides absolute yields for UV fluxes higher than 10^{13} photons s^{-1} .

The UHV set-up is connected to the undulator-based FUV beamline DESIRS at the SOLEIL synchrotron facility in Saint-Aubin (France). In a first irradiation mode, the photon beam from the undulator stage is used directly. The high harmonics of the photon energy are filtered using a rare-gas filled chamber,

Table 1
Energy-dependent Photodesorption Rates for 10 ML Thick CO Ice at 18 K

Irradiation Energy (eV)	Relative Rate ($\text{cm}^{-1}(\text{photons cm}^{-2})^{-1}$)	Absolute Rate ($\text{molecules photon}^{-1}$)
8.2	2.19×10^{-19}	$2.8 \pm 1.7 \times 10^{-2}$
9.2	1.07×10^{-19}	$1.3 \pm 0.91 \times 10^{-2}$
10.2	0.54×10^{-19}	$6.9 \pm 2.4 \times 10^{-3}$
11.2	0.74×10^{-19}	$9.3 \pm 3.4 \times 10^{-3}$

set in the pass of the UV beam. Absolute incident photon fluxes are measured using calibrated photodiodes. This setting yields high photon flux (10^{14} photons s^{-1}) at selected energies with a well-defined photon energy distribution (Lorentzian with FWHM of 1 eV). Irradiations at fixed photon energies (8.2, 9.2, 10.2, and 11.2 eV) are performed to monitor the CO ice loss with photon fluence using RAIR spectroscopy (see Figure 1). These experiments are used to derive absolute photodesorption rates for different spectral windows where CO ice absorption is known to differ (see Section 3.1).

In a second irradiation mode, the photons enter a 6.65 m normal incidence monochromator equipped with a 200 grooves mm^{-1} grating. In this configuration, a photon flux up to 10^{12} photons s^{-1} with a resolution of 40 meV at 10 eV for a 700 μm exit slit is achieved. The CO ice film is then irradiated by photons whose energy is linearly increased throughout the experiment, from 7 to 13.6 eV (90 to 170 nm). A relative photodesorption rate spectrum is obtained by recording the QMS signal of desorbing CO while tuning the photon energy (see the upper panel of Figure 2 and Section 3.2).

3. RESULTS

3.1. Absolute Photodesorption Yields for 1 eV Spectral Windows

Figure 1 shows the decrease of the CO stretching feature during irradiation of a 10 ML thick ice at 18 K by 9.2 eV photons at a flux of 1.2×10^{14} photons s^{-1} . The double-peaked structure of the infrared feature does not change during ice growth and is most likely due to the roughness of the gold substrate; the peak structure is known to be sensitive to the arrangement of adsorbed molecules on the surface (Palumbo et al. 2006). The evolution of the CO absorption band integrated area as a function of photon fluence is shown in the inset. The integrated band area is directly proportional to the amount of CO ice (from RAIR spectra acquired during ice growth). The loss of integrated band area during irradiation can therefore be used to quantify CO desorption.

The observed linear relationship between CO ice integrated area and photon fluence is consistent with a zeroth-order process, similar to what has been seen for broadband irradiation experiments (Öberg et al. 2007; Muñoz Caro et al. 2010). This zeroth-order kinetics is observed for the four explored irradiation energies (8.2, 9.2, 10.2, and 11.2 eV) until the ice coverage gets below 0.03 cm^{-1} integrated absorbance (~ 6 ML). The same effect has been observed by Muñoz Caro et al. (2010). Fitting straight lines to the linear parts of the ice loss at the four investigated irradiation energies provides energy-dependent photodesorption yields.

The results from the fits are summarized in Table 1. The relative photodesorption yields (absorbance per incident photon flux) are converted into absolute photodesorption yields (CO molecules per incident photon) using the absorbance to ML

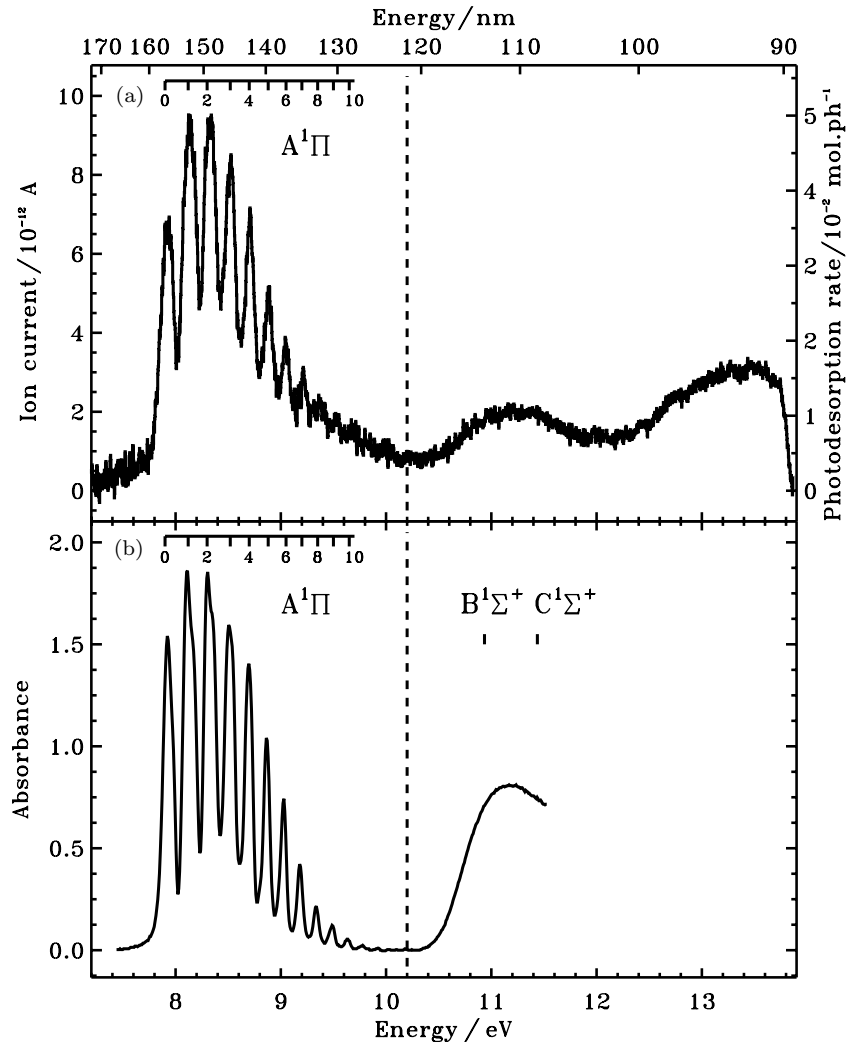


Figure 2. (a) Photodesorption spectrum (after background subtraction) of a 10 ML CO ice at 18 K using a resolution of 40 meV (at 10 eV) and a scan step of 12 meV every 0.5 s. (b) Absorption spectrum of solid CO at 10 K (Lu et al. 2005). The dashed line indicates photodesorption and absorption values at Ly α , 121.6 nm.

conversion factor for the present RAIRS set-up (Section 2) and assuming that 1 ML = 10^{15} molecules cm^{-2} . The uncertainties in the relative yields are due to the intrinsic RAIRS measurement uncertainties. The larger uncertainties on the absolute yields are due to ice thickness calibration and to differences in the FUV irradiated area versus IR probed area. Indeed, the sample area probed by the IR beam and the UV-beam spot at the surface are $1 \pm 0.1 \text{ cm}^2$ and $0.7 \pm 0.1 \text{ cm}^2$, respectively. Caution has been taken to ensure that the UV irradiated area is integrally probed by the IR beam. The photodesorption yields vary between 6.9 and 28×10^{-3} molecules photon^{-1} for the investigated energy range and are thus clearly wavelength-dependent. The lowest yield is obtained at 10.2 eV, which is important considering that previous photodesorption results were based on broadband UV discharge lamps, which are often dominated by photons at this excitation energy. In addition, the strong variation with photon energy motivates a more detailed investigation on the energy dependence of the photodesorption yield.

3.2. CO Photodesorption Yield Spectrum

A detailed investigation of the wavelength dependence is achieved in the second kind of experiment, where a 10 ML thick CO ice sample is irradiated by a monochromatic photon

beam scanning 7–13.6 eV at a constant rate, while probing photodesorption with the QMS. The QMS current resulting from the desorbing gas phase CO ($m/z = 28$) versus photon energy is presented in Figure 2 together with a UV absorption spectra of CO ice from Lu et al. (2005). This photodesorption spectrum is converted into molecules photon^{-1} using the absolute photodesorption yields, obtained from the first series of experiments (Section 3.1, Table 1). The scaling takes into account the exact spectral profiles in the 1 eV spectral-window experiments, which was monitored carefully for the 8.2 eV window. Figure 2(a) shows that when probed at a high spectral resolution, the photodesorption yield varies even more across the investigated energy range compared to the 1 eV spectral-window measurements. The lowest yield is achieved below 7.8 eV and at 10.2 eV ($<6 \times 10^{-3}$ molecules photon^{-1}) and it is an order of magnitude lower than the peak value of 5×10^{-2} molecules photon^{-1} at ~ 8.2 eV. The average UV profile below 10 eV results in a total photodesorption yield of 1.8×10^{-2} molecules photon^{-1} . This value is a factor of seven higher than the previously reported yield of 2.7×10^{-3} molecules photon^{-1} from Öberg et al. (2009), and comparable within a factor of two to the yield of 3.5×10^{-2} molecules photon^{-1} found by Muñoz Caro et al. (2010). The relative contribution of Ly α photons (and their inefficiency

at inducing photodesorption) to the total photon flux in each experiment is a probable origin for the different yields, further stressing the importance of wavelength resolved studies.

4. DISCUSSION

4.1. Mechanism

The photodesorption spectrum (Figure 2(a)) has a band structure below 10 eV that is almost identical to the absorption spectrum of pure CO ice obtained by Lu et al. (2005). The observed spectral progression is attributed to the transition from CO ground state to vibrational levels of the first allowed electronic state ($A^1\Pi$). The striking similarity between the two spectra provides the first experimental evidence that desorption is a DIET (Desorption Induced by Electronic Transition) process, as previously suggested by Öberg et al. (2007, 2009). Desorption of condensed molecules is probably induced by subsequent relaxation of the excited molecules via energetic transfer from electronic to vibrational degrees of freedom (Avouris & Walkup 1989). This process clearly dominates the spectrum below 10 eV. Above 10 eV, the main photodesorption mechanism is expected to be more complex since the second absorption band of CO is dissociative. In this case, photodesorption may result from several relaxation pathways, including chemical recombination and desorption, as proposed in the case of water (Westley et al. 1995; Watanabe et al. 2000; Arasa et al. 2010).

It should be noted that electrons, resulting from the interaction of incident UV photons with the metallic substrate, may also contribute to the observed CO ice desorption. Most of the UV photons can be absorbed by the metallic substrate since the ice coverage is an order of magnitude below the coverage limit for which most of the photons would be absorbed by the ice before reaching the substrate. Hot electrons resulting from electron-hole pair excitation of gold are expected to be produced for all investigated irradiation energies and may induce desorption (e.g., Bonn et al. 1999). Free electrons photo-emitted from the gold substrate may also induce CO desorption by electronic excitation or resonant electron attachment (Schultz 1973; Rakhovskaia et al. 1995; Shi et al. 1998; Mann et al. 1995). Only photons whose energy is above 10 eV can produce secondary free electrons energetic enough to trigger the latter process, since the CO-covered gold surface work function is ~ 4.4 eV (Gottfried et al. 2003). The importance of these electron-induced processes can be estimated from our experiment, since the production of electrons (primary photoelectrons and inelastically diffused secondary electrons) that have enough kinetic energy to trigger the CO desorption process within the ice, should increase with the photon energy. This effect is barely observed; electrons are most likely the cause of the low-level continuously increasing desorption background seen in Figure 2(a). In other words, DIET is the main pathway leading to the observed photodesorption below 10 eV, resulting in a strong energy dependence of the photodesorption yields.

4.2. Astrophysical Implications

The determined strong wavelength dependence of the photodesorption yield of CO ice presented in Figure 2(a) demonstrates that the CO photodesorption yield is expected to vary significantly in different astrophysical environments. Incorporating this information into astrochemical networks is important to accurately predict the partitioning of CO between the gas and ice. Table 2 exemplifies how this wavelength-dependent data can be used to predict the photodesorption efficiency in sources

Table 2
CO Photodesorption in Different ISM Environments

Environment (molecules photon ⁻¹)	Yield	References for UV profile
Edges of clouds	1.2×10^{-2}	Mathis et al. (1983)
Pre-stellar cores	9.4×10^{-3}	Gredel et al. (1987)
Black body 10,000 K	1.6×10^{-2}	van Dishoeck et al. (2006)
Tw Hydrae	6.6×10^{-3}	Bergin et al. (2003)
Pure Ly α	4.1×10^{-3}	121.6 nm

with characteristic UV fields. The listed photodesorption yields have been calculated by convolving UV field profiles from the literature with the CO photodesorption spectrum presented in Figure 2(a) between 90 and 180 nm. The UV profiles are the ISRF from Mathis et al. (1983) appropriate to model the UV field at the edges of molecular clouds, an emission spectrum of cosmic-ray-excited H₂ (Gredel et al. 1987) to mimic UV field encountered in cloud cores, a 10,000 K black body for the UV field around an Herbig Ae star (van Dishoeck et al. 2006) and the emission of TW Hydrae from Bergin et al. (2003) to illustrate photodesorption in protoplanetary disks. Pure Ly α is also added for comparison. The calculated characteristic photodesorption yields vary by a factor of four, with the lowest yields around T Tauri stars and other environments where the UV field is dominated by Ly α photons, and the highest yields per incident photon at cloud edges and next to a 10,000 K black body. The photodesorption yields used here are valid for pure CO ice thicker than ~ 6 ML, as stated in Section 3.1. How the CO photodesorption efficiency and mechanism change with ice thickness and/or composition should certainly be studied in order to extend the applicability of the present results to thinner pure CO ices or mixed CO containing astrophysical ices.

It is important to note that the UV spectral profile deeper into the cloud and disk may be radically different compared to the UV field incident on the cloud and disk surface because of wavelength-dependent radiative transfer. Determining accurate interstellar relevant photodesorption yields requires a combination of photodesorption spectrum and detailed UV radiative transfer. In the meantime, the presented photodesorption spectrum is recommended to calculate photodesorption yields for specific environments (Table 2).

5. CONCLUSIONS

This study provides the first photodesorption spectrum of pure CO ice, obtained by tunable synchrotron UV irradiation of CO ice under astrophysically relevant conditions. A quantitative determination of the photodesorption yields at 8.2–13.6 eV has been achieved by the simultaneous probe of the ice- and gas-phase CO concentrations coupled to either narrowband (1 eV) excitation mode at selected energies or to continuous energy scanning by monochromatic UV radiation. The resulting photodesorption yields vary by an order of magnitude over the investigated wavelength range. The CO photodesorption process is dominated by the direct electronic excitation of the condensed CO molecules (DIET) below 10 eV. Other desorption mechanisms involving secondary electrons due to UV interactions with the substrate are present, but their contributions to the total measured desorption yield are minor. Consistent with a DIET mechanism, the photodesorption yield of CO ice at Ly α is low. This may result in different chemical evolutions in regions where the UV field is dominated by line emission compared to regions where the UV emission is due to black body radiation. The

calibrated photodesorption spectrum presented here should therefore be used to determine the characteristic CO ice photodesorption yields by convolving the CO photodesorption spectrum to the UV profile found in a specific astrophysical environment. In general, the link between wavelength-dependent UV absorption of the ice and the resulting photodesorption and photochemistry is key to implement astrochemical gas-grain models and should be experimentally investigated for relevant ice species.

We are grateful to Ewine van Dishoeck and Marc van Hemert for stimulating discussions. We thank Hsiao-Chi Lu, Roland Gredel, and Edwin Bergin for providing useful data. We acknowledge SOLEIL for provision of synchrotron radiation facilities, as well as Laurent Nahon for technical help on the beamline DESIRS. Financial support from the French national program PCMI (Physique chimie du milieu interstellaire), the Dutch program NOVA (Nederlandse Onderzoekschool Voor Astronomie), the COST action CM0805 “The Chemical Cosmos,” and the Hubert Curien Partnership “Van Gogh,” are gratefully acknowledged. Support for K.I.Ö is provided by NASA through a Hubble Fellowship grant awarded by the Space Telescope Science Institute, which is operated by the Association of Universities for Research in Astronomy, Inc., for NASA, under contract NAS 5-26555.

REFERENCES

- Arasa, C., Andersson, S., Cuppen, H. M., van Dishoeck, E. F., & Kroes, G.-J. 2010, *J. Chem. Phys.*, **132**, 184510
- Avouris, P., & Walkup, R. E. 1989, *Annu. Rev. Phys. Chem.*, **40**, 173 (and references therein)
- Bergin, E., Calvet, N., D’Alessio, P., & Herczeg, G. J. 2003, *ApJ*, **591**, L159
- Bertin, M., Romanzin, C., Michaut, X., Jeseck, P., & Fillion, J.-H. 2011, *J. Phys. Chem. C*, **115**, 12920
- Bonn, M., Funk, S., Hess, Ch., et al. 1999, *Science*, **285**, 1042
- Gottfried, J. M., Schmidt, K. J., Schroeder, S. L. M., & Christmann, K. 2003, *Surf. Sci.*, **536**, 206
- Gredel, R., Lepp, S., & Dalgarno, A. 1987, *ApJ*, **323**, L137
- Greenberg, L. T. 1973, in IAU Symp. 52, *Interstellar Dust and Related Topics*, ed. J. M. Greenberg & H. C. van de Hulst (Dordrecht: Reidel), **3**
- Lu, H.-C., Chen, H.-K., Cheng, B.-M., Kuo, Y.-P., & Ogilvie, J. F. 2005, *J. Phys. B: At. Mol. Opt. Phys.*, **38**, 3693
- Mann, A., Cloutier, P., Liu, D., & Sanche, L. 1995, *Phys. Rev. B*, **51**, 7200
- Mathis, J. S., Mezger, P. G., & Panagia, N. 1983, *A&A*, **128**, 212
- Muñoz Caro, G. M., Jiménez-Escobar, A., Martín-Gago, J. A., et al. 2010, *A&A*, **522**, A108
- Öberg, K. I., Fuchs, G. W., Awad, Z., et al. 2007, *ApJ*, **662**, L23
- Öberg, K. I., van Dishoeck, E. F., & Linnartz, H. 2009, *A&A*, **496**, 281
- Palumbo, M. E., Baratta, G. A., Collings, M. P., & McCoustra, M. R. S. 2006, *Phys. Chem. Chem. Phys.*, **8**, 279
- Pontoppidan, K. M., Fraser, H. J., Dartois, E., et al. 2003, *A&A*, **408**, 981
- Rakhovskaia, O., Wiethoff, P., & Feulner, P. 1995, *NIM B*, **101**, 169
- Schulz, G. J. 1973, *Rev. Mod. Phys.*, **45**, 423
- Shi, H., Cloutier, P., & Sanche, L. 1998, *Low Temp. Phys.*, **24**, 742
- van Dishoeck, E. F., Bastiaan, J., & van Hemert, M. C. 2006, *Faraday Discuss.*, **133**, 231
- Watanabe, N., Horii, T., & Kouchi, A. 2000, *ApJ*, **541**, 772
- Westley, M. S., Baragiola, R. A., Johnson, R. E., & Baratta, G. A. 1995, *Nature*, **373**, 405
- Willacy, K., & Langer, W. D. 2000, *ApJ*, **544**, 903